



On the influence of ENSO complexity on Pan-Pacific coastal wave extremes

Julien Boucharel^{a,b,1} , Rafael Almar^c, Elodie Kestenare^c, and Fei-Fei Jin^{b,1} 

^aLaboratoire d'Etudes en Géophysique et Océanographie Spatiales, CNRS, University Paul Sabatier, Toulouse 31400, France; ^bDepartment of Atmospheric Sciences, School of Ocean & Earth Science & Technology, University of Hawai'i at Mānoa, Honolulu, HI 96822; and ^cLaboratoire d'Etudes en Géophysique et Océanographie Spatiales, IRD, University Paul Sabatier, Toulouse 31400, France

Edited by Anny Cazenave, Centre National d'Etudes Spatiales, Toulouse, France, and approved October 12, 2021 (received for review August 26, 2021)

Wind-generated waves are dominant drivers of coastal dynamics and vulnerability, which have considerable impacts on littoral ecosystems and socioeconomic activities. It is therefore paramount to improve coastal hazards predictions through the better understanding of connections between wave activity and climate variability. In the Pacific, the dominant climate mode is El Niño Southern Oscillation (ENSO), which has known a renaissance of scientific interest leading to great theoretical advances in the past decade. Yet studies on ENSO's coastal impacts still rely on the oversimplified picture of the canonical dipole across the Pacific. Here, we consider the full ENSO variety to delineate its essential teleconnection pathways to tropical and extratropical storminess. These robust seasonally modulated relationships allow us to develop a mathematical model of coastal wave modulation essentially driven by ENSO's complex temporal and spatial behavior. Accounting for this nonlinear climate control on Pan-Pacific wave activity leads to a much better characterization of waves' seasonal to interannual variability (+25% in explained variance) and intensity of extremes (+60% for strong ENSO events), therefore paving the way for significantly more accurate forecasts than formerly possible with the previous baseline understanding of ENSO's influence on coastal hazards.

ENSO | coastal waves | seasonal forecasts | atmospheric teleconnections | nonlinear climate system

As coastal breaking waves represent the ultimate dissipation of the energy generated by local and remote storms through large increases in surface wind over the ocean, their activity is modulated by the large-scale ocean–atmosphere coupled variability. This emphasizes the importance of better understanding the connections between coastal dynamics and modes of climate variability in order to improve their prediction at subseasonal timescales and beyond (1, 2). In particular, the Pacific basin is under the siege of El Niño Southern Oscillation (ENSO), the strongest interannual climate fluctuation, which has widespread effects on weather, climate, and societies (3). Recently, the littoral community has started to identify the role of ENSO as a major driver of coastal vulnerability across the Pacific (4, 5). The alternating coastal conditions, with shifts in wave activity and water-level anomalies between the northeastern and northwestern Pacific, were noted to mimic the well-known oscillations of ENSO phases. However, the Pacific wave climate and coastal variability associated with ENSO remains only understood at a basic reconnaissance level (6). As a matter of fact, even the most recent studies on the connection between wave climate and coastal extremes have only relied on a simplified view of ENSO (7, 8), omitting the existence of different regimes with distinct teleconnections and dynamics, recently coined “ENSO diversity and/or complexity” (9, 10).

“ENSO diversity” originates from the concept that Sea Surface Temperature (SST) anomaly patterns exhibit wide variations. In particular, the repeated occurrence of SST patterns in the central Pacific (CP) in the 2000s suggested that ENSO events may be grouped into two flavors: the conventional El Niño, with SST anomalies concentrated in the eastern Pacific

(EP El Niño), and the CP El Niño, with SST anomalies located around the dateline (11, 12). The “complexity” or sometimes “diversity and complexity” further refers to ENSO's irregular temporal behavior characterized by large variations in amplitude and duration. In particular, recent progresses demonstrated that ENSO's seasonal phase locking (i.e., its tendency to peak in boreal winter) (13) can produce a low-frequency instability known as the “Annual cycle-ENSO combination mode” and generate a deterministic variability at near-annual timescales, which significantly broadens the ENSO continuum (14). Such diversity and complexity translate to pronounced differences in remote ENSO climate impacts on the climate system through atmospheric and oceanic teleconnections (15, 16). In particular, one of ENSO's most significant influences is its modulation of Tropical Cyclone (TC) activity, one of the most severe natural hazards (17). Because the large-scale air–sea environment mostly drives these storms, TC activity is substantially modified by ENSO through atmospheric and oceanic pathways (18). Similarly, ENSO also strongly affects extratropical storms and related coastal wave activity (19, 20).

A variety of oceanic and atmospheric wave reanalysis products and TC databases were examined to capture comprehensively the regional and large-scale climate variability in the Pacific associated with ENSO diversity and complexity and how it affects coastal waves' variability. More specifically and unlike any previous studies, the focus is not solely directed toward the direct influence on extratropical wave patterns of El Niño at its winter peak but also on its delayed and early effects on summer TC storminess considered as an integral wave regime

Significance

This study demonstrates how the main wave regimes in the Pacific, in particular related to tropical and extratropical storm activity, are activated by different El Niño/Southern Oscillation (ENSO) teleconnections patterns. By combining these robust relationships with the latest theoretical advances in ENSO research, a mathematical model of wave energy modulation is derived. It allows a better representation of wave extremes over a range of time scales wider than previously possible with the previous baseline understanding of ENSO's influence on coastal impacts. This paves the way for unprecedented seasonal to monthly forecasts of coastal hazards around the densely populated Pacific basin.

Author contributions: J.B. and R.A. designed research; J.B. performed research; J.B. and F.-F.J. contributed new reagents/analytic tools; E.K. provided the data; J.B. and R.A. analyzed data; and J.B. wrote the paper.

The authors declare no competing interest.

This article is a PNAS Direct Submission.

Published under the [PNAS license](#).

¹To whom correspondence may be addressed. Email: bouch@hawaii.edu or jff@hawaii.edu.

This article contains supporting information online at <http://www.pnas.org/lookup/suppl/doi:10.1073/pnas.2115599118/-DCSupplemental>.

Published November 15, 2021.

potentially affecting coastlines far from the storms' generation (21). In particular, since ENSO's influences on tropical and extratropical storm activity are subject to a strong seasonal synchronization, the combined ENSO–Annual cycle influence on teleconnections patterns and coastal wave variability is considered. Insights from these unraveled seasonally modulated ENSO teleconnections allow us to develop a simple mathematical model that points toward a strong predictability of the Pacific coastal wave variability over a range of timescales much broader than just the interannual band and therefore opens up the door for predictions of coastal hazards significantly more accurate than current state-of-the-art seasonal forecasts.

The ENSO-Modulated Extratropical Storminess and Coastal Wave Variability in Winter

First, we evaluate the connections between coastal wave variability at select sites across the Pacific basin and storm activity during the boreal winter. The extratropical storminess is diagnosed as the interannual anomalies of 14-d high-pass-filtered daily eddy kinetic energy (EKE) at the 850-mb pressure level. Fig. 1 *A* and *B* present the regression of EKE onto interannual anomalies of daily wave energy in the central eastern (Hawaii) and western (Philippines) Pacific, respectively, over the period 1979 to 2016. An increased wave energy in the Philippines is associated with the strengthening of the polar jet stream concurrently with a reinforcement of easterlies in the central equatorial and northeastern tropical Pacific typically observed during La Niña (Fig. 1*A*). Conversely, an increased coastal wave activity on the other side of the basin is related to an increased (decreased) jet stream activity in the subtropical (polar) regions along with an enhanced equatorial high-frequency wind activity related to westerly wind bursts, a well-known kickstarting and maintaining feature of El Niño events (Fig. 1*B*). This analysis showcases the ENSO winter teleconnections to the northern hemisphere jet stream activity. It highlights in particular the atmospheric bridge linking changes in ENSO tropical background to changes in extratropical storminess.

To investigate the large-scale pathways behind this ENSO's winter teleconnection to the northern Pacific extratropical storminess, Fig. 1 *C* and *D* present regression patterns between interannual anomalies of wave energy in the west (Philippines) and in the central-east tropical Pacific (Hawaii) and various environmental variables. As expected, the winter wave activity in the Philippines is significantly increased during ENSO cold phases as evidenced by the SST regression pattern typical of La Niña, marked by colder (warmer) SST in the central eastern (western) equatorial Pacific (shading in Fig. 1*C*). This oceanic signature promotes an enhanced winter monsoon anticyclonic circulation strengthening the polar jet stream, characterized by stronger northeasterly winds/swells (Fig. 1*C*, arrows) in the western subtropical Pacific (22). Conversely, the winter wave activity in Hawaii (and California; *SI Appendix*, Fig. S3*C*) is significantly augmented during EP El Niño events as indicated by warm SST anomalies in the eastern equatorial Pacific (shading Fig. 1*D*) and related westerly wind anomalies in the central equatorial Pacific (arrows Fig. 1*D*). This leads to a stronger Aleutian low-pressure system and the equatorward displacement of the polar jet (19). This strengthened storm track produces large northwesterly swells battering Hawaii (and California; cf. *SI Appendix*, Fig. S4 *C* and *D*) shores during El Niño boreal winters and which are energetic enough to reach South America's coastlines (Peru; *SI Appendix*, Fig. S5 *G* and *H*).

The ENSO-Modulated TC Activity and Coastal Wave Variability in Summer

We now establish the connections between coastal wave variability and the different Pacific TC basin activity controlling the

strength of summer tropical storms. TC storminess is diagnosed as the interannual anomalies of daily accumulated cyclone energy (ACE), which represents an integrated measure of the basin-scale tropical storm activity (23). Summer wave energy in the Philippines is increased concurrently with a stronger (weaker) tropical storm activity in the north (south) western Pacific TC basin (Fig. 1*C*), a pattern reminiscent of the CP El Niño imprint on TC variability (18). In Japan, coastal wave variability is coherent with a TC activity decreased along the East Asian seaboard and increased in the center of the western Pacific basin, a signature typical of EP El Niño events (*SI Appendix*, Fig. S4*E*). Wave energy in Hawaii (Fig. 1*D*) is related to a southward displacement of tropical storm activity evocative of the EP El Niño influence in the EP basin (18, 24). This analysis demonstrates the strong control of ENSO on coastal wave variability in boreal summer through its complex regional imprint on the basin-scale TC activity.

To further examine the large-scale controls related to different types of ENSO's teleconnections to the northern Pacific TC activity, Fig. 1 *G* and *H* present regression patterns between interannual anomalies of summer wave energy across the Pacific and various oceanic and atmospheric variables. This analysis confirms that the Philippines wave activity in boreal summer is activated by teleconnection patterns linked to CP El Niño. The SST regression (Fig. 1*G*) features an equatorial warming on the dateline flanked on each side by colder water, typical of this ENSO flavor. This oceanic pattern initiates an enhanced cyclonic circulation accompanied by a strong dipole of vertical wind shear (VWS) in the northwestern tropical Pacific (0 to 30° N, 120 to 150° E) that resembles the dipole of convective anomalies triggered by the ENSO influence on the Boreal Summer Intra Seasonal Oscillation (25) and leads to a northward shift of favorable background atmospheric conditions for TC genesis during the summer onset of CP El Niño (18, 20). This in turn increases wave activity over Japan and the Philippines.

The summer wave energy in the northeastern Pacific (Hawaii and California) is increased during El Niño's decay and transition toward La Niña. Fig. 1*H* highlights the off-equatorial heat discharge responsible for this ENSO phase shift according to the well-known "recharge paradigm" (26). Despite an atmospheric environment (VWS) barely favorable for TC genesis, this meridional redistribution of heat can favor the occurrence of major TCs during seasons following the peak of El Niño (24). These TCs, either westward traveling or northward reclining, can generate swells affecting Hawaii or California, respectively. The ENSO phase transition also promotes a reinforcement of the Inter Tropical Convergence Zone (~25°N) and an increase in summer northeast trade wind swells. This summer wave variability associated with ENSO teleconnections to regimes of TC activity occurring at different stages of the cycle and for different types of events is likely to complicate the simplified "ENSO dipole picture" of alternating winter coastal hazards across the Pacific (4, 5).

Seasonal Impacts of ENSO Diversity on Coastal Waves Variability across the Pacific

We now quantify how much these different seasonal ENSO teleconnection pathways contribute to significant changes in extreme wave occurrence in the Pacific. Fig. 2 presents, for select locations across the basin and different ENSO flavors/phases, the percentage of days within a season characterized by a wave energy and period above one SD of their interannual anomalies. Results using the 95th percentile of significant wave height as a more drastic threshold to characterize extremes are presented and discussed in *SI Appendix*. Winter wave activity (January to March) in the north Pacific follows the EP ENSO

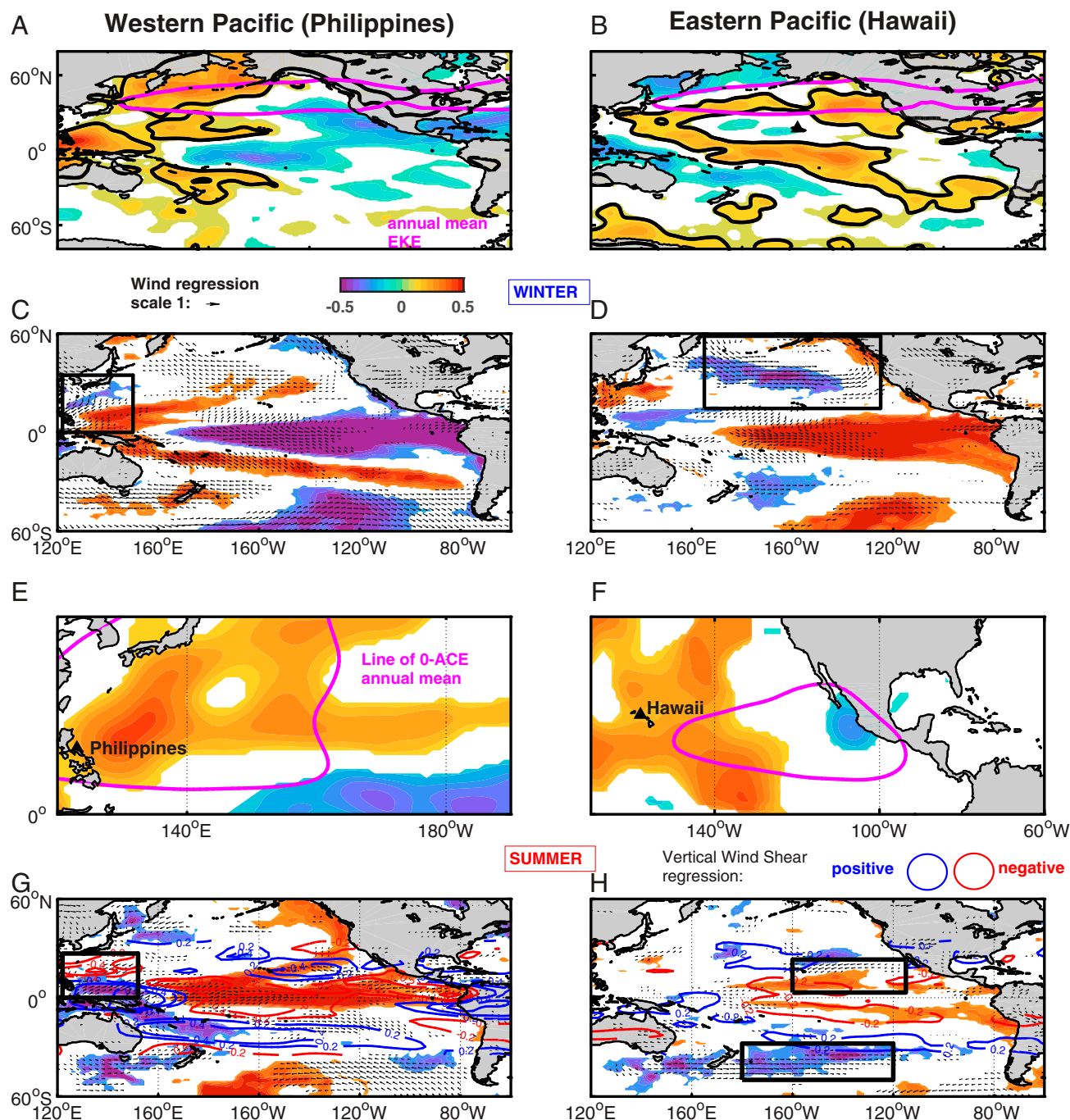


Fig. 1. Coastal wave activity and ENSO teleconnection to seasonal storm regimes. The extratropical storminess in winter: regression of interannual anomalies of 14-d high-pass-filtered daily EKE at the 850 mb pressure level onto interannual anomalies of winter daily wave energy in the western (Philippines, A) and central eastern (Hawaii, B) Pacific. (Upper) Magenta contours represent the average position of the 850 hPa jet stream (iso-contour of $3 \times 10^7 \text{ m}^2 \cdot \text{s}^{-2}$). Regressions of wave energy interannual anomalies onto environmental variables: SST (shading), wind direction and amplitude (arrows) in the boreal winter in the central eastern (Hawaii, C) and western Pacific (Philippines, D). The tropical storm activity in summer: regression of interannual anomalies of daily ACE onto interannual anomalies of summer daily wave energy in the western (Philippines, E) and central eastern (Hawaii, F) Pacific. (Lower) Magenta contours represent the 0-line of mean ACE. Regressions of wave energy interannual anomalies onto environmental variables: SST (shading), wind direction and amplitude (arrows), and VWS anomalies (blue/red contours) in the boreal summer in the central eastern (Hawaii, G) and western Pacific (Philippines, H).

oscillating pattern manifested by increased/reduced wave energy (by almost threefold) in the east during El Niño/La Niña events and the opposite behavior in the west (cf. Fig. 2 A and C versus Fig. 2 E and G). Although not as pronounced and restricted to the tropics, there is a similar seesaw across the Pacific in the occurrence of extreme winter waves between La

Niña and CP El Niño events. This flavor also promotes an increase in wave energy in the northwestern Pacific (Fig. 2G).

Remarkably, wave extremes follow a similar, yet out of phase, swinging pattern across the Pacific in summer. The onset of El Niño (most notably the CP flavor) stimulates an increase in large waves in the western Pacific, up to twofold as compared

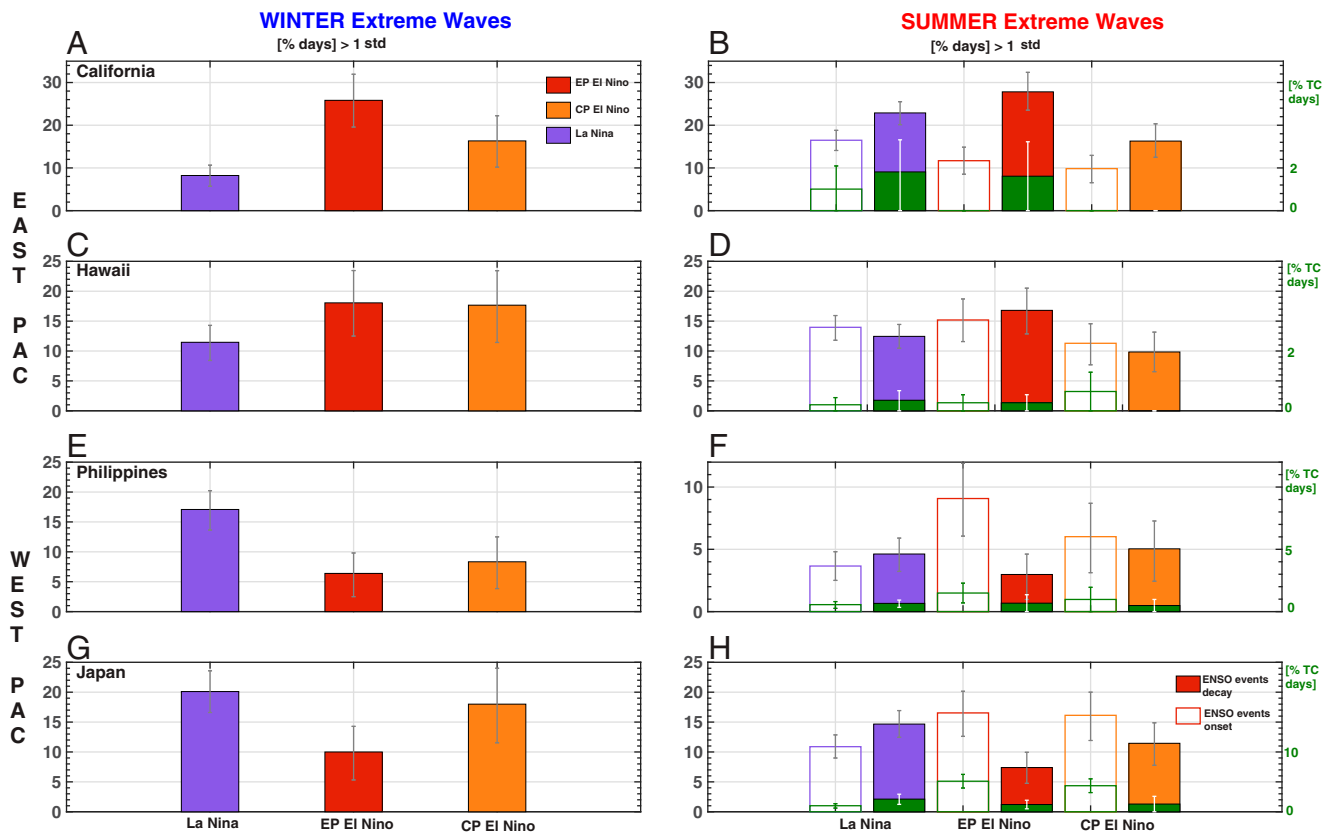


Fig. 2. ENSO flavors and seasonal extreme wave occurrence. Percentage of occurrence of extreme wave days (above one SD, “1 std,” of the interannual period and wave energy anomalies) depending on ENSO phases and types in winter (January to March, *Left*) and summer (June to September, *Right*) at different locations in the Eastern Pacific (EAST PAC) (California and Hawaii, *Top*) and in the western Pacific (WEST PAC) (Philippines and Japan, *Lower*). Hollow (filled) bars are for summers preceding (following) the peak of the events, that is, the onset (decay) phase of El Niño. Note that the green bars indicate the fraction of swell days originating only from TC in summer (with a different green y-axis on the *Right*). Error bars indicate the 5 to 95% quantile range.

to the summer development of La Niña (see Fig. 4 *F* and *H*, hollow color bars). This increase in wave activity is partly due to the enhanced cyclonic activity in the western basin during boreal summers preceding both types of El Niño events (cf. previous section). Meanwhile, in the EP, we observe an increase in large summer waves through La Niña’s development (only significant compared to CP events). Interestingly, this oscillating pattern reverses again during the summertime decay of CP El Niño. The meridional heat discharge of EP events and subsequent transition toward La Niña, which drive an increase in trade winds and TC swells in the EP (yet not significant for cyclonic waves), extend this seesaw pattern into the summer. The clear reduction of extreme waves in the western Pacific after the peak of EP El Niño is attributed to the decrease in TC activity during El Niño decay (solid bars on Fig. 2 *F* and *H*) (27, 28).

To illustrate spatially the different seasonal oscillating coastal wave variability around the Pacific basin associated with ENSO diversity, Fig. 3 features composite maps of daily wave energy anomalies throughout the cycle of the two ENSO flavors. In particular, the top/middle panels present composites averaged during the summer onset (Fig. 3 *A* and *D*), winter peak (Fig. 3 *B* and *E*), and summer decay (Fig. 3 *C* and *F*) of EP/CP El Niño events, respectively. The rightmost panel is the composite during La Niña’s boreal winter peak (Fig. 3*G*). The buildup of EP events features a moderate seesaw in wave energy anomalies across the basin, positive (negative) in the west (east). This pattern sharply reverses and intensifies at the peak of El Niño, lingers during the decay phase, before reversing abruptly again at the peak of La Niña. In contrast, the onset of CP events is already characterized by a strong dipole of positive (negative)

wave energy anomalies in the western (eastern) Pacific that progressively reverses at the peak of the event. This pattern reverses again during the CP El Niño decay and intensifies until the following La Niña.

A Mathematical Model of the Seasonal to Interannual Modulation of Pan-Pacific Coastal Wave Variability

This study documents two major seasonal wave regimes in the Pacific, namely the tropical and extratropical storminess, and how they are activated by different ENSO teleconnection pathways. The strong difference in coastal wave variability–ENSO relationship between summer and winter suggests that wave energy should be well captured by indices of ENSO flavors and their nonlinear seasonal modulation via the “annual-cycle/ENSO combination mode” (14). Similarly, to Boucharel and Jin’s consideration for tropical instability waves (29), we apprehend the occurrence of coastal wave events as an oscillating weather phenomenon (i.e., a transient of the climate system) characterized by an amplitude modulation that responds nonlinearly to slow climate forcing: that is, ENSO and the tropical Pacific annual cycle. By extending their theory, we formulate the following model of the Pan-Pacific wave energy Z :

$$\frac{dZ}{dt} = \left[-\left(\gamma_0 + \frac{2i\pi}{T} \right) + m(t) \right] Z(t) + \omega(t),$$

where γ_0 is the wave energy damping rate or decorrelation time (i.e., 10 d^{-1} ; cf. *SI Appendix*, Fig. S8 *B* and *C*), T the approximate average return periods of wave events ($T = 15 \text{ d}$), and $m(t)$ and $\omega(t)$ the deterministic and stochastic climate forcing,

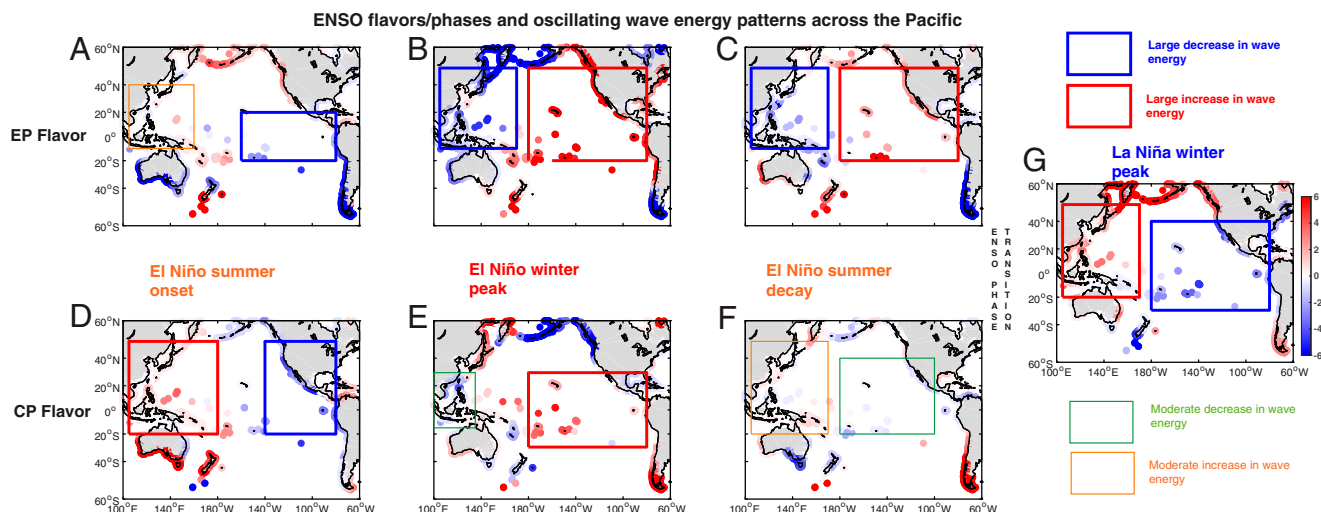


Fig. 3. Oscillating coastal wave activity around the Pacific Rim in relation with ENSO flavors. Composite maps of daily wave energy (in square meters per second [m^2s], colored dots) anomalies averaged during the boreal summer onset (June to September, A and D), winter peak (January to March, B and E), and summer decay (June to September, C and F) of EP/CP El Niño events. The rightmost panel is the composite during the boreal winter peak of La Niña events (G). The classification and seasonality of the different ENSO flavors are detailed in the methodology section. Red (orange) boxes indicate regions marked by strongly (moderately) increased coastal wave activity; blue (green) boxes delineate regions marked by strongly (moderately) decreased coastal activity.

respectively. $\omega(t)$ is a white noise with an amplitude a 10th of the forcing term $m(t)$, which can be formulated as follows:

$$m(t) = \left[\gamma_A \cos \frac{2\pi(t - \phi)}{T_A} \right] + [\gamma_C C_{mode} + \gamma_E E_{mode}].$$

The first term represents the annual cycle forcing with T_A and ϕ the annual cycle period (12 mo) and phase, respectively. ϕ is chosen so that the annual cycle amplitude reaches a maximum in January/February and a minimum in July/August ($\phi=2$) similarly to the ENSO amplitude cycle in order to account for the ENSO seasonal phase-locking effect on the Pacific storminess and coastal wave variability. The second term represents the interannual forcing related to ENSO diversity. We choose two uncorrelated, independent ENSO indices E_{mode} and C_{mode} , accounting for the two ENSO flavors, respectively, the EP and CP El Niño, as the first two rotated principal components of the decomposition of SST interannual anomalies into Empirical Orthogonal Functions (30).

Using this theoretical framework, we first evaluate the part of stochastic versus deterministically forced variability of the seasonal to interannual modulation of coastal wave activity. To quantify the range of the stochastic variability related to the randomness of storm generation, we generate a 50-member ensemble, each member numerically integrated with a fourth-order Runge–Kutta method. We present in Fig. 4 results from two main sites across the Pacific (California and the Philippines). The ensemble average of the interannual modulation of wave energy activity (or amplitude, i.e., the 2-mo running mean of wave energy) yields remarkable correlations with reanalysis data (0.63 and 0.57 for California and the Philippines, respectively; cf. Fig. 4 A and D). Most of the seasonal to interannual variability of coastal wave activity in California and the Philippines falls within the range of stochastic variability with some notable exceptions. Interestingly, we noticed that these exceptions were more likely to happen in summer, which we interpret as either an increase in TC genesis randomness and/or wave variability related to other climate modes not accounted for by this formalism, in particular from the Southern Annular Mode (SAM), dominant in boreal summer and that can affect the Pacific eastern seaboard on the form of remote long-period swells originating from the Southern Ocean. Indeed, we

observe a strong connection between California/Hawaii's summer wave activity and the Southern Hemisphere jets, characterized by a strengthening of the subtropical jet along a disappearance of the polar jet (cf. Fig. 1H and SI Appendix, Fig. S4) indicative of the SAM locked in its negative phase during the boreal summer (31).

We now quantify the respective contributions of different forcing time scales to the deterministic variability and amplitude of coastal wave activity. To do so, we rely on the simplicity of this mathematical formalism, which allows deriving the analytical solution of the wave energy amplitude modulation (23). The stochastic variability of the analytical solution (toward which converges the simulations' ensemble mean) is smoothed out so that this solution only accounts for the deterministically forced variability. The second-order analytical solution of low-frequency coastal wave amplitude $|Z^2|$ can be then written as follows:

$$|Z^2| = K e^{-\gamma_0} \left[1 + \frac{m(t)}{\gamma_0} + \frac{m^2(t)}{\gamma_0^2} \right].$$

The analytical solutions of interannual anomalies of coastal wave amplitude yield correlation with the reanalysis similar to the numerical solutions ensemble means (0.68 and 0.61 for California and the Philippines, respectively; cf. thick red lines in Fig. 4 A and D). The reconnaissance level at which the coastal wave activity associated with ENSO is understood is essentially only contained in the direct linear forcing term EP El Niño (4–8), which basically represents the canonical ENSO mode. Our approach goes further and allows us to quantify the variance explained by the different forcing terms of the solution, 1) the direct/linear ENSO forcing $[\gamma_C C_{mode} + \gamma_E E_{mode}]$ and 2) the nonlinear interactions between the climate forcing contained in $m^2(t)$. In particular, we quantify a 25% (respectively, 20%) increase in explained coastal wave variability in California (respectively, the Philippines) between the linear solution that accounts only for the direct effect of the EP mode ($\gamma_E E_{mode}$; Fig. 4 A and D) and the total solution (accounting for the full diversity and complexity of ENSO). In addition, we observe a substantial improvement in the intensity of extremes: that is, +70% (+50%) during strong El Niño (La Niña) events in California (the Philippines). This increase can be explained in

Model of Wave Energy modulation

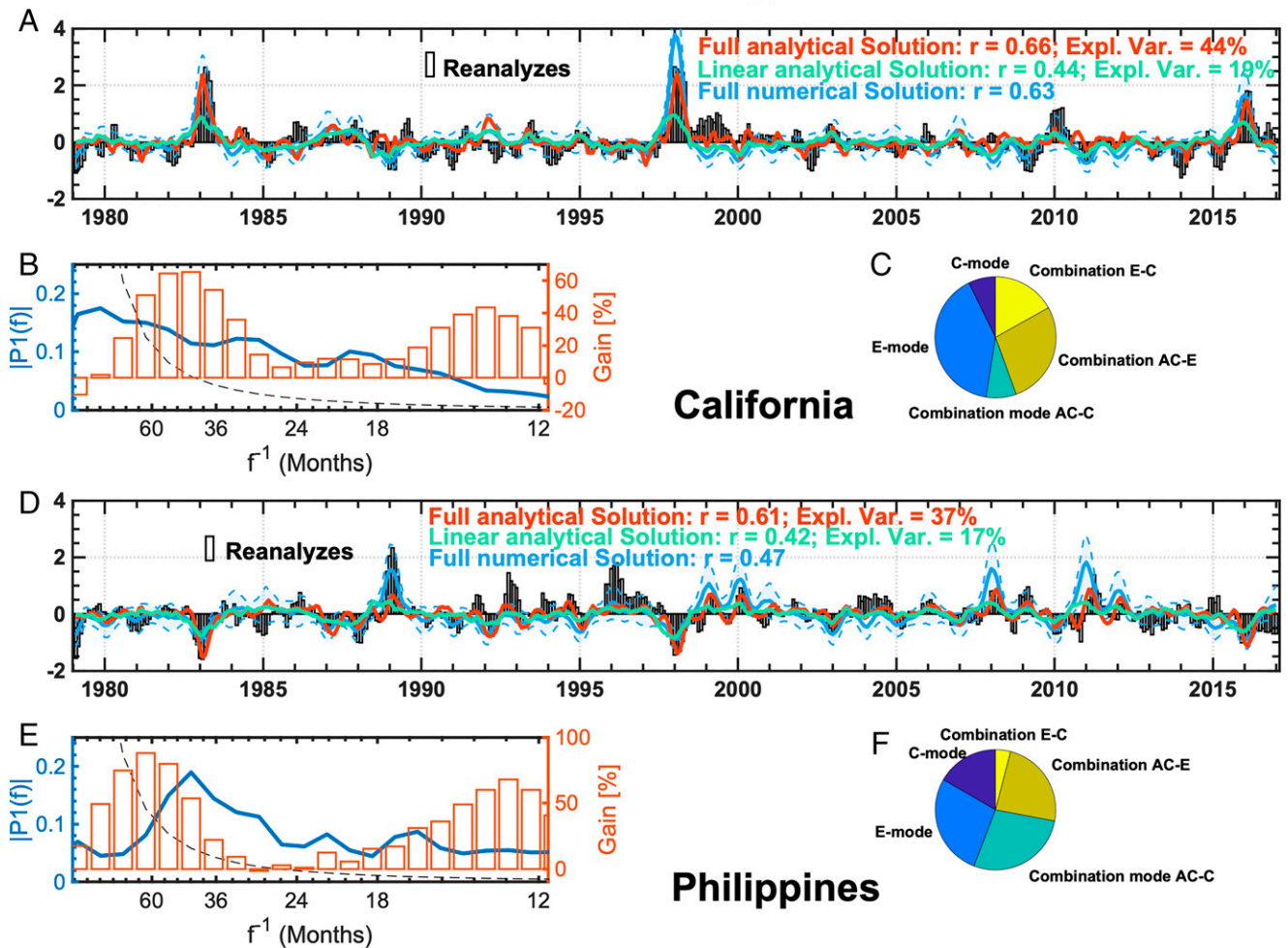


Fig. 4. Model of seasonal to interannual modulation of wave energy. Reanalysis (bars), ensemble average of the 50-member numerical solutions (thick blue line, the thin, dashed blue lines represent plus and minus 1 SD of the ensemble), total model analytical solution (red lines), and analytical solution restricted to the linear EP El Niño forcing (green line) of normalized 2-mo smoothed monthly anomalies of wave energy in the eastern (California, *A*) and western (Philippines, *D*) Pacific. Spectrum of the 2-mo smoothed monthly anomalies of wave energy reanalysis (blue lines) in the eastern (California, *B*) and western (Philippines, *E*) Pacific. The orange bars represent the gain (in percentage) in spectral power between the total analytical solution and the solution restricted to the EP El Niño linear forcing compared to the reanalysis. The pie charts represent the respective contributions of the different linear and nonlinear (combination modes) deterministic forcing terms to the total analytical solution in the eastern (California, *C*) and western (Philippines, *F*) Pacific.

particular by a better representation of the interannual variability including both the EP and CP ENSO modes (30 to 80 mo^{-1}) and their nonlinear interactions with the annual cycle (the combinations modes), manifested at the resonant frequencies $f = f_{\text{Annual Cycle}} \pm f_{\text{ENSO}}$, the dominant one being at 14 to 18 mo^{-1} (cf. Fig. 4 *B* and *E*). Interestingly, a strong part of the coastal wave interannual variability is explained by the EP (respectively, CP) El Niño mode and its combination with the annual cycle in the eastern (respectively, western) part of the basin (cf. Fig. 4 *C* and *F*).

Implications for Coastal Wave-Induced Hazard Forecasts in the Pacific Basin

Our simple mathematical model provides insights into the non-linear climate connection to the deterministic coastal wave variability in the Pacific by embedding a variety of dynamical pathways from the diverse ENSO background states down to the tropical and extratropical storminess into a simple theoretical framework (cf. Fig. 5). Therefore, we believe these findings

can point toward the development of new forecast models of wave and associated coastal hazards variability around the densely populated Pacific Rim over a range of timescales much wider than just the interannual El Niño signal (the benchmark so far in coastal impacts predictions in the Pacific). Such simple tools appear increasingly necessary to interpret the newest generation of high-resolution wave climate projections and reanalysis products that integrate all the intrinsic complexity and nonlinearity of the planetary climate forcing in particular related to the multifaceted ENSO mode.

Methods

Wave and Atmospheric Data. Surface winds and wave data (significant height H_s , peak period T_p , and direction) are extracted from the European Centre for Medium-Range Weather Forecasts (ECMWF) Re-Analysis version 5 (ERA-5) at a 3-h temporal resolution between 1979 and 2016 and a $0.5^\circ \times 0.5^\circ$ horizontal resolution (32). Wave energy is defined as $H_s^2 T_p$.

In particular, to cover most of the Pacific basin's wave conditions, we extract and analyze the following seven locations:

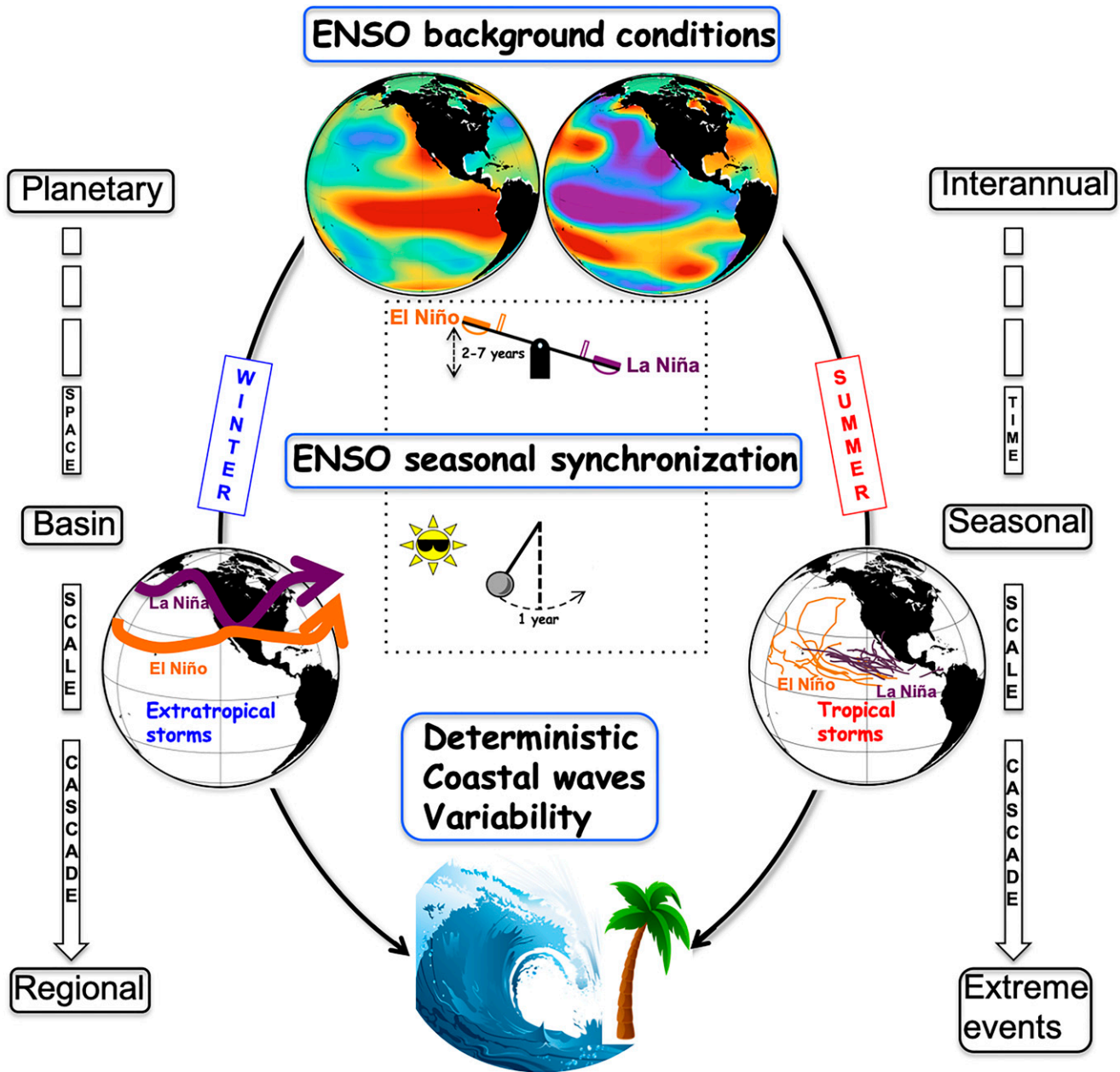


Fig. 5. Schematic diagram illustrating ENSO seasonal pathways to deterministic coastal wave activity in the Pacific basin. ENSO's alteration of background climate conditions leads to seasonally distinct coastal wave variability through a spatiotemporal scale cascade originating from the nonlinear interactions between ENSO frequencies and the annual cycle.

- California (32.5° N; 242° E)
- Hawaii southeast (17.3° N; 207° E)
- Hawaii northwest (17.5° N; 207° E)
- Japan (34.5° N; 140° E)
- Philippines (14.5° N; 123° E)
- Eastern Australia (34.5° S; 154° E)
- Peru (11.5° N; 282° E).

Note that in order to avoid local coastal effects, such as swell dissipation or refraction, we chose to extract the wave data in the open ocean (~100 km off the coast). Two locations are chosen for Hawaii to make sure to capture both north and south/cyclonic swells that might stay otherwise in the Islands' shadows. We use the Hawaiian northwest or, respectively, southeast location to capture the wintertime or, respectively, summertime ENSO teleconnections between large-scale environmental variability and the local wave climate. This is motivated by the dominance of winter swells originating mostly from the high latitude (northwest of the islands) and summer trade wind, cyclonic swells from the tropics as well as swells from the Southern Hemisphere (southeast of the islands).

To make sure that wind-wave coupled bias internal to the ERA products do not reverberate on our analysis, we also compare ERA waves to atmospheric reanalysis data from the National Center for Environmental Prediction-National Center for Atmospheric Research (33). The VWS, one of the most commonly used environmental variables to assess the environmental control of TC genesis and intensity (34), is defined as the horizontal wind difference between 200- and 850-hPa pressure levels (35).

Oceanic Data. The SST is taken from the ECMWF Ocean Reanalysis System 4 (36). All variables are either daily, monthly, or yearly averaged, and interannual anomalies are computed with respect to a monthly mean climatology.

TC Data. Tracks and intensities of TC are extracted over the same period of 1979 to 2016 from the best track archives provided by the National Oceanographic and Atmospheric Administration's (NOAA's) Tropical Prediction Center. To evaluate TC activity, we use a spatial density index. The storm annual density is the yearly number of TCs with maximum sustained winds larger than 32 kn in a $5 \times 5^\circ$ sliding box covering the entire Pacific basin at a $1 \times 1^\circ$ resolution (23).

Identification of Swells Originating from TC. TCs have been shown to modulate coastal vulnerability in regions that are not under their direct influence, that is, regions that did not undergo landfalls, through the generation of energetic cyclonic waves (21). To disentangle coastal waves that have a cyclonic source from waves generated by local trade winds or high-latitudes storms, we use a backtracking procedure (21). We briefly describe the methodology's main steps.

- Step 1:
We first isolate days when coastal waves display the following characteristics:
 - Swell peak period $T_p > 11$ s. This criterion allows discarding local low-energy swells (i.e., wind waves) with little coastal impacts (37).
 - Interannual anomaly (relative to a monthly climatology) of wave energy (i.e., $H_s T_p$) above one SD, calculated over the TC season only (June to October in the Northern Hemisphere and January to March for the Southern Hemisphere).
- Step 2:
Once we have estimated all significant waves events at a given location that can potentially originate from a TC (i.e., passed step 1), we evaluate for each of them if at least one TC occurred in the corresponding TC basin the same day and up until 7 d before the wave episode at the chosen location.
- Step 3:
We use a backtracking procedure to assess if the position of one of these storms could explain the wave event characteristics at the coastal location. To do so, we define eight different regions of the possible location of the storm that generates such swells the same day, the day before, and up until 7 d before the wave event occurs at the coast (based on maximum lags evidenced in Fig. 1). These cone-shaped regions are delineated using three dimensions: the cone height, its angle, and its orientation relative to the zonal line passing through the location. The height represents the maximum distance potentially traveled by the swell in 1 d and is estimated using the wave peak period T_p of the waves at the coastal location and the deep-water approximation [$\sim (1.56T_p)/2$, c being the swell propagation speed, that is, the group speed, and T_p the swell peak period]. The orientation parameter is simply the wave event direction at the coast. We use an angle (15°) that represents an uncertainty parameter supposed to account for the swell dissipation and the TC travel along the normal to the incoming swell direction.

Storm Activity (i.e., Storminess).

Extratropical storms. Winter storms are mostly conveyed by midlatitude jet streams, that is, the zonally nonuniform narrow current of strong winds in the midtroposphere between 850 and 250 hPa. Jet streams are strongly influenced by atmospheric Rossby waves on 1- to 2-wk time scales (38). Therefore, to characterize the jet-stream activity that affects oceanic surface waves, we decide to use the EKE of 14-d high-pass-filtered winds at the 850 hPa pressure level (lower troposphere).

$$EKE = \frac{1}{2} [U_*^2 + V_*^2], \quad [1]$$

with

$$\begin{cases} U_* = U_{@850hPa}[14 - \text{days Highpass}] \\ V_* = V_{@850hPa}[14 - \text{days Highpass}] \end{cases} \quad [2]$$

To assess the modulation of extratropical storm activity, we compute the 60-d smoothed interannual EKE daily anomalies (with respect to a monthly mean climatology).

Tropical storms. As an integrated measure of TC activity, we use the ACE index. First, ACE is calculated for individual TC as the sum of the squares of the 1-min maximum sustained surface wind speeds >35 kt over all 6 h periods during a storm's lifetime (39). The ACE accounts for both TC frequency and intensity. After calculating all storms' ACE, an ACE-gridded product is computed similarly to storm density (see above).

To assess the modulation of tropical storm activity, we compute the 60-d smoothed interannual ACE daily anomalies (with respect to a monthly mean climatology).

Both EKE and ACE have been spatially smoothed using a two-dimensional $3^\circ \times 3^\circ$ Gaussian filter.

Classification of ENSO Events. ENSO events are chosen according to the Climate Prediction Center classification. Boreal (austral) winter composites are for January to March (June to August) period. Boreal (austral) summer composites are for June to September (January to March) period.

EP El Niño years: 1983, 1987, 1988, 1992, 1998, and 2016.

CP El Niño years: 1991, 1996, 2003, 2005, and 2010.

La Niña years: 1984, 1985, 1989, 1990, 1996, 1997, 1999, 2000, 2002, 2008, 2009, 2011, 2012, and 2013.

Summer onset years are the events' years minus 1. Summer decay years are the same events' years.

Statistical Test. A bootstrap method was conducted for the significance test of Fig. 4. The 95% percentile confidence level is carried out by the outer 5 and 95% of the bootstrap sampling distribution generated by repeatedly taking random samples from the observation dataset with 10,000 times replacement. Other statistical tests are based on a classic Student's t test.

Model of Coastal Wave Energy. The model is based on the stochastically forced model of fast climate variability introduced by Hasselmann and Frankignoul and Hasselmann (40, 41).

We have also tested this model with more conventional ENSO indices as forcing terms characteristic of the EP and CP flavors, respectively, the classic Niño3 and Niño4 indices, which are calculated as the spatial average of SST anomalies in the 90° to 150° W, 5° N to 5° S or, respectively, 160° E to 150° W, 5° N to 5° S region.

Boucharel and Jin (29) showed that it is possible to derive the analytical solution of the modulation of $Z = H_s^2 T_p$ as long as the transient's period T is much lower than climate forcing's periods. *SI Appendix, Fig. S8A* shows the Welch power spectra of this model's climate forcing. Besides the obvious peak at 12 mo (i.e., T_A) indicative of the annual cycle, we observe different peaks for the different ENSO mode forcing terms, in particular $T_{ENSO1} \sim 55$ mo, $T_{ENSO2} \sim 26$ mo, $T_{ENSO3} \sim 18$ mo (for the E-index), and $T_{ENSO4} \sim 130$ mo and $T_{ENSO4} \sim 40$ mo (for the C-index). *SI Appendix, Fig. S8 B and C* illustrate the decorrelation time scales of wave energy in California (~ 11 d) and Japan (~ 7 d), respectively. The former is mostly under the influence of high-latitude winter storms, while the latter is majorly influenced by summer tropical storms. This unambiguously indicates that $T \ll T_A$ and $T \ll T_{ENSO}$. This estimation of the wave energy decorrelation time represents also the wave energy damping rate, that is, γ_0^{-1} .

Since our model resembles Linear Inverse Models (42, 43), we can obtain the remaining forcing terms' coefficients (γ_A, γ_C , and γ_E) and therefore the full analytical solution through a multilinear regression of the wave energy inter-annual modulation onto the different ENSO indices and the annual cycle.

This model of wave activity, if used in a forecast mode, could offer lead time equivalent to state-of-the-art ENSO forecasts (i.e., ~ 3 to 6 mo) (44) and therefore valuable anticipation for littoral and islands' communities particularly vulnerable in this part of the world.

Spectral Analysis. We estimate the power spectral density $|P(f)|$, of the input signal (i.e., either the observations or the analytical solutions of the wave energy anomalies modulation), using a Welch's overlapped segment averaging estimator (using three segments with 50% overlap).

Data Availability. Previously published data were used for this work (Copernicus Climate Change Service [C3S] ERA5: Fifth generation of ECMWF atmospheric reanalyses of the global climate). Copernicus Climate Change Service Climate Data Store (CDS), date of access November 1, 2021. ERA5 data can be freely downloaded via the Copernicus portal (<https://cds.climate.copernicus.eu/cdsapp#!/dataset/reanalysis-era5-single-levels?tab=overview>).

ACKNOWLEDGMENTS. J.B. is funded by the French Agence Nationale de la Recherche project Make Our Planet Great Again "Trocodyn" (ANR-17-MPGA-0018) and the Région Occitanie. F.-F.J. is supported by US NSF (AGS-1813611) and Department of Energy (DE-SC0005110).

1. L. Mentaschi, M. I. Vousdoukas, E. Voukouvalas, A. Dosio, L. Feyen, Global changes of extreme coastal wave energy fluxes triggered by intensified teleconnection patterns. *Geophys. Res. Lett.* **44**, 2416–2426 (2017).
2. R. J. Nicholls, A. Cazenave, Sea-level rise and its impact on coastal zones. *Science* **328**, 1517–1520 (2010).
3. M. J. McPhaden, S. E. Zebiak, M. H. Glantz, ENSO as an integrating concept in earth science. *Science* **314**, 1740–1745 (2006).

4. P. L. Barnard et al., Extreme oceanographic forcing and coastal response due to the 2015–2016 El Niño. *Nat. Commun.* **8**, 14365 (2017).
5. P. Barnard et al., Coastal vulnerability across the Pacific dominated by El Niño/Southern Oscillation. *Nat. Geosci.* **8**, 801–807 (2015).
6. T. R. Mortlock, I. D. Goodwin, Impacts of enhanced central Pacific ENSO on wave climate and headland-bay beach morphology. *Cont. Shelf Res.* **120**, 14–25 (2016).

7. I. Odériz *et al.*, Natural variability and warming signals in global ocean wave climates. *Geophys. Res. Lett.* **48**, e2021GL093622 (2021).
8. I. Odériz, R. Silva, T. R. Mortlock, N. Mori, El Niño-Southern Oscillation impacts on global wave climate and potential coastal hazards. *J. Geophys. Res. Oceans* **125**, e2020JC016464 (2020).
9. A. Capotondi *et al.*, Understanding ENSO diversity. *Bull. Am. Meteorol. Soc.* **96**, 921–938 (2015).
10. A. Timmermann *et al.*, El Niño-Southern Oscillation complexity. *Nature* **559**, 535–545 (2018).
11. H. Kao, J. Yu, Contrasting eastern-Pacific and central-Pacific types of ENSO. *J. Clim.* **22**, 615–632 (2009).
12. J.-S. Kug, F.-F. Jin, S.-I. An, Two-types El Niño: Cold tongue El Niño and warm pool El Niño. *J. Clim.* **22**, 1499–1515 (2009).
13. K. Stein, A. Timmermann, N. Schneider, F.-F. Jin, M. F. Stuecker, ENSO seasonal synchronization theory. *J. Clim.* **27**, 5285–5310 (2014).
14. M. Stuecker *et al.*, A combination mode of the annual cycle and the El Niño/Southern Oscillation. *Nat. Geosci.* **6**, 540–544 (2013).
15. A. S. Taschetto *et al.*, “ENSO atmospheric teleconnection” in *El Niño Southern Oscillation in a Changing Climate*, M. McPhaden, A. Santoso, W. Cai, Eds. (American Geophysical Union, 2020), vol. **253**, p. 311–336.
16. J. Sprintall, S. Cravatte, B. Dewitte, Y. Du, A. S. Gupta, “ENSO oceanic teleconnections” in *El Niño Southern Oscillation in a Changing Climate*, M. J. McPhaden, A. Santoso, W. Cai, Eds. (2020).
17. P. B. Peduzzi *et al.*, Global trends in tropical cyclone risk. *Nat. Clim. Chang.* **2**, 289–294 (2012).
18. I.-I. Lin *et al.*, “ENSO and tropical cyclones” in *El Niño Southern Oscillation in a Changing Climate*, M. McPhaden, A. Santoso, W. Cai, Eds. (American Geophysical Union, 2020), vol. **253**, p. 377–408.
19. R. Seager, N. Harnik, Y. Kushnir, W. Robinson, J. Miller, Mechanisms of hemispherically symmetric climate variability. *J. Clim.* **16**, 2960–2978 (2003).
20. H.-M. Kim, P. J. Webster, J. A. Curry, A modulation of North Pacific tropical cyclone activity by three phases of ENSO. *J. Clim.* **24**, 1839–1849 (2011).
21. R. Almar, E. Kestenare, J. Boucharel, On the key influence of the remote climate variability from Tropical Cyclones, North and South Atlantic mid-latitude storms on the Senegalese coast (West Africa). *Env. Res. Commun.* **1**, 071001 (2019).
22. R. Zhang, A. Sumi, M. Kimoto, Impact of El Niño on the East Asian monsoon: A diagnostic study of the '86/87 and '91/92 events. *J. Meteorol. Soc. Jpn.* **74**, 49–62 (1996).
23. J. Boucharel, F.-F. Jin, M. H. England, I. I. Lin, Modes of hurricane activity variability in the eastern Pacific: Implications for the 2016 season. *Geophys. Res. Lett.* **43**, 11–358 (2016).
24. F.-F. Jin, J. Boucharel, I. I. Lin, Eastern Pacific tropical cyclones intensified by El Niño delivery of subsurface ocean heat. *Nature* **516**, 82–85 (2014).
25. H. Lin, Long-lead ENSO control of the boreal summer intraseasonal oscillation in the East Asian-western North Pacific region. *npj Clim. Atmos. Sci.* **2**, 31 (2019).
26. F. F. Jin, An equatorial ocean recharge paradigm for ENSO. Part I: Conceptual model. *J. Atmos. Sci.* **54**, 811–829 (1997).
27. J. C. L. Chan, Tropical cyclone activity in the northwest Pacific in relation to the El Niño/Southern Oscillation phenomenon. *Mon. Weather Rev.* **113**, 599–606 (1985).
28. Y. Du, L. Yang, S.-P. Xie, Tropical Indian Ocean influence on northwest Pacific tropical cyclones in summer following strong El Niño. *J. Clim.* **24**, 315–322 (2011).
29. J. Boucharel, F.-F. Jin, A simple theory for the modulation of tropical instability waves by ENSO and the annual cycle. *Tellus A Dyn. Meteorol. Oceanogr.* **72**, 1–14 (2020).
30. K. Takahashi, A. Montecinos, K. Goubanova, B. Dewitte, ENSO regimes: Reinterpreting the canonical and Modoki El Niño. *Geophys. Res. Lett.* **38**, L10704 (2011).
31. F. Codron, Relations between annular modes and the mean state: Southern hemisphere winter. *J. Atmos. Sci.* **64**, 3328–3339 (2007).
32. H. Hersbach *et al.*, The ERA5 global reanalysis. *Q. J. R. Meteorol. Soc.* **146**, 1999–2049 (2020).
33. S. Saha *et al.*, The NCEP climate forecast system. *J. Clim.* **19**, 3483–3517 (2006).
34. S. J. Camargo, A. H. Sobel, A. G. Barnston, P. J. Klotzbach, “The influence of natural climate variability on tropical cyclones, and seasonal forecasts of tropical cyclone activity” in *Global Perspectives on Tropical Cyclones*, J. C. I. Chan, J. D. Kepert, Eds. (2010), pp. 325–360.
35. M. DeMaria, The effect of vertical shear on tropical cyclone intensity change. *J. Atmos. Sci.* **53**, 2076–2088 (1996).
36. M. A. Balmaseda, K. Mogensen, A. T. Weaver, Evaluation of the ECMWF ocean reanalysis system ORAS4. *Q. J. R. Meteorol. Soc.* **139**, 1132–1161 (2013).
37. M. Sadio *et al.*, Shoreline changes on the wave-influenced Senegal River delta, West Africa: The roles of natural processes and human interventions. *Water* **9**, 357 (2017).
38. A. Gill, *Atmosphere-Ocean Dynamics* (Academic Press, New York, 1982), p. 662.
39. G. D. Bell *et al.*, Climate assessment for 1999. *Bull. Am. Meteorol. Soc.* **81**, S1–S50 (2000).
40. K. Hasselmann, Stochastic climate models Part I. Theory. *Tellus* **28**, 473–485 (1976).
41. C. Frankignoul, K. Hasselmann, Stochastic climate models, Part II. Application to sea-surface temperature anomalies and thermocline variability. *Tellus* **29**, 289–305 (1977).
42. C. Penland, L. Matrosova, A balance condition for stochastic numerical models with application to the El Niño–Southern oscillation. *J. Clim.* **7**, 1352–1372 (1994).
43. C. Penland, P. D. Sardeshmukh, The optimal growth of tropical sea surface temperature anomalies. *J. Clim.* **8**, 1999–2024 (1995).
44. M. L. L’Heureux *et al.*, “ENSO predictions” in *El Niño Southern Oscillation in a Changing Climate*, M. McPhaden, A. Santoso, W. Cai, Eds. (American Geophysical Union, 2020), vol. **253**, p. 377.